Molecular Crystals and Liquid Crystals
Publication details, including instructions for authors and subscription information:
http://www.informaworld.com/smpp/title~content=t713644168

Molecular Orientation of a Nematic Between Concentric Cylinders: Weak Anchoring Situation

C. A. R. Yednak[ab]; R. Teixeira de Souza[a]; G. G. Lenzi[ac]; E. K. Lenzi[ab]; L. R. Evangelista[a]
[a] Departamento de Física, Universidade Estadual de Maringá Avenida Colombo, Maringá (PR), Brazil [b] Dipartimento di Fisica, Politecnico di Torino, Corso Duca degli Abruzzi, Torino, Italy [c] DISMIC - Dipartimento di Scienza dei Materiali e Ingegneria Chimica, Politecnico di Torino, Corso Duca degli Abruzzi, Torino, Italy

First published on: 19 August 2010

To cite this Article Yednak, C. A. R. , de Souza, R. Teixeira , Lenzi, G. G. , Lenzi, E. K. and Evangelista, L. R.(2010) 'Molecular Orientation of a Nematic Between Concentric Cylinders: Weak Anchoring Situation', Molecular Crystals and Liquid Crystals, 526: 1, 82 — 92
To link to this Article: DOI: 10.1080/15421406.2010.485076
URL: http://dx.doi.org/10.1080/15421406.2010.485076

Mol. Cryst. Liq. Cryst., Vol. 526: pp. 82–92, 2010

ISSN: 1542-1406 print/1563-5287 online
DOI: 10.1080/15421406.2010.485076

Taylor & Francis
Taylor & Francis Group

Molecular Orientation of a Nematic Between Concentric Cylinders: Weak Anchoring Situation

C. A. R. YEDNAK,[1,2] R. TEIXEIRA DE SOUZA,[1]
G. G. LENZI,[1,3] E. K. LENZI,[1,2] AND
L. R. EVANGELISTA[1]

[1]Departamento de Física, Universidade Estadual de Maringá Avenida Colombo, Maringá (PR), Brazil
[2]Dipartimento di Fisica, Politecnico di Torino, Corso Duca degli Abruzzi, Torino, Italy
[3]DISMIC – Dipartimento di Scienza dei Materiali e Ingegneria Chimica, Politecnico di Torino, Corso Duca degli Abruzzi, Torino, Italy

The molecular orientation of a nematic sample limited by two concentric cylinders is theoretically investigated. The surfaces are assumed as having an inhomogeneous distribution of easy directions. The results are found in the one-constant approximation, in the presence of an external electric field, for weak anchoring of the molecules at the surfaces. In order to validate our approximations, the analytical results are compared with the ones obtained by numerically solving the non-linear bulk differential equation for the tilt angle profile subjected to non-linearized boundary conditions. We show that the agreement improves as the extrapolation length increases.

Keywords Dirichlet-Neumann problem; Fréedericksz transition; inhomogeneous easy axes; weak anchoring

PACS Numbers 61.30.Gd; 61.30.Hn; 61.30.Pq

I. Introduction

The director profile of a nematic liquid crystal (NLC) in cylindrical geometry is a classical problem investigated by several authors [1–6]. Very recently, a generalization of this problem was presented in the strong anchoring situation [7], by considering also that the surfaces impose inhomogeneous distribution of easy directions. In the framework of the elastic continuum theory, the determination of the equilibrium profile of the director in the situation of strong anchoring on the boundaries corresponds to the Dirichlet's problem, whereas the weak anchoring situation leads to the mixed Dirichlet – Neumann problem [8–10]. In this work, we re-examine the problem by taking into account the presence of an external electric field, parallel to the cylinder

Address correspondence to L. R. Evangelista, Departamento de Física, Universidade Estadual de Maringá Avenida Colombo, 5790-87020-900, Maringá (PR), Brazil. Tel.: 55 44 3011 5905; Fax: 55 44 3263 4623; E-mail: Lrevang@gmail.com

radius, in the limit of small distortions and in the situation of weak anchoring at the surfaces. We are thus facing the Dirichlet–Newmann problem, which constitutes a much more difficult mathematical problem, but a more realistic physical situation. Another motivation for re-examining the problem, in the framework of the usual approximations of one-elastic constant, parabolic form of the surface energy [11], and small distortions regime, is to obtain analytical solutions for the director profile in a mathematical formulation as general as possible. These analytical results can be also used to investigate the limitations of this kind of approach. In fact, for checking the validity of these approximations, we report some results obtained by means of numerical calculations, using Runge-Kutta method to solve the non-linearized boundary-value problem. In this latter case, in which the mentioned approximations are absent, the complete differential equation, together with the non-linear boundary conditions, must be faced in order to solve the problem. Nevertheless, the results of this comparison do not invalidate the approximated approach; on the contrary, they reinforce the conclusion that the approximations, usually adopted, are formally correct and constitute a useful tool to analytically solve difficult boundary-value problems in the context of elastic theory of NLC.

II. Statement of the Problem

The sample is a nematic liquid crystal cell limited by two concentric cylinders of radii a and $b > a$, whose cylindrical reference frame is such that the z axis is parallel to the cylinder axes, as shown in Figure 1 and discussed in more details in Ref. [7]. The geometry of the problem is such that the director is given by $\mathbf{n} = \cos[\psi(\rho,\theta,z)]\cos[\phi(\rho,\theta,z)]\hat{e}_\rho + \sin[\psi(\rho,\theta,z)]\cos[\phi(\rho,\theta,z)]\hat{e}_\theta + \sin[\phi(\rho,\theta,z)]\hat{e}_z$, where $\hat{e}_\rho = \cos(\theta)\hat{e}_x + \sin(\theta)\hat{e}_y$, $\hat{e}_\theta = -\sin(\theta)\hat{e}_x + \cos(\theta)\hat{e}_y$ and $\hat{e}_z = \hat{e}_z$. In what follows, we will consider the director as remaining in the polar plane, implying that only ψ can assume non-vanishing values and that the director can be considered z-independent. Because the molecules are weakly anchored at the surfaces, the director can take on directions different from the ones imposed by the easy axes. Moreover, we consider that the easy directions are not uniform, i.e., the surfaces favor a θ-dependent deformation, and the easy axes vary point-to-point at the boundaries in an inhomogeneous way. For this reason, the tilt angle depends on ρ and θ.

As stated above, to analytically face the problem, we assume that the distortions are small. In this manner, our approach is valid for an applied field whose intensity is near to the one defined by the Fréedericksz threshold field. The anisotropic dielectric constant $\varepsilon_a = \varepsilon_\parallel - \varepsilon_\perp < 0$, (where $\parallel$ and $\perp$ refer to the direction of $\mathbf{n}$) plays a very

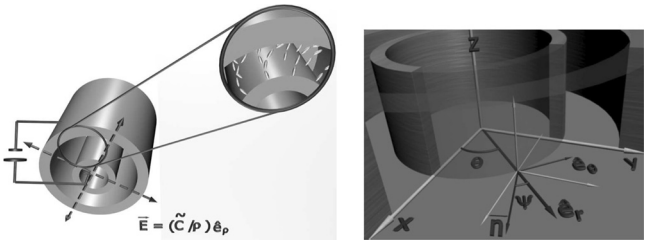

Figure 1. Nematic sample limited by two concentric cylinders of radius a and b. A ρ-dependent electric field is directed along a radial direction (normal to the cylinder axes, $\hat{e}_z$). The director angle ψ is also shown for a hypothetical distortion in the polar plane.

important role in this context [3,6]. The coupling term between the electric field and the nematic director is given by $\varepsilon_a(\mathbf{E}\cdot\mathbf{n})^2/2$; thereby, parallel directions of $\mathbf{E}$ and $\mathbf{n}$ are privileged if this value is positive; the opposite situation is expected if ε_a is negative. Particular attention should be paid to work with the director in the weak anchoring situation. If the field is much strong, the surface orientation can be dismantled. However, when the anchoring energy is finite, but the anchoring is still strong enough for not be destroyed by the external field (which should be strong enough to orient the molecules in the polar plane), the problem can be solved. The electric field considered here appears when the surfaces of the sample, located at $\rho = a$ and $\rho = b$, are subjected to a constant potential difference. A typical situation is achieved when the surface $\rho = a$ is subjected to an electric potential $\varphi = V/2$ and the surface $\rho = b$ to an electric potential $\varphi = -V/2$. For this case, after solving the Maxwell equations, one obtains that $\mathbf{E} = (\widetilde{\mathcal{C}}/\rho)\mathbf{e}_\rho$ with $\widetilde{\mathcal{C}} = V/\ln(b/a)$. Since liquid crystals are anisotropic media, the electric susceptibility can be a function of the tilt angle and may have a spatial dependence in the form

$$\varepsilon(\rho,\theta) = \varepsilon_\perp + \varepsilon_a \sin^2\psi(\rho,\theta). \tag{1}$$

Therefore, there is a coupling between the molecular orientation and the electric field [12]; consequently, the field inside the sample may differ a little from the one given above. In fact, the electric displacement vector, which gives de real field into the sample, is written as

$$\mathbf{D} = \varepsilon(\rho,\theta)\mathbf{E}. \tag{2}$$

However, in the small distortions regime, in which the value of the field must remain near to the Freédericksz threshold one, this coupling is usually small and can be neglected.

In the one-constant approximation, i.e., $K_{11} = K_{22} = K_{33} = K$, the total elastic free energy per unit length along the z axis is given by

$$\begin{aligned} F[\psi(\rho,\theta)] = &\int_0^{2\pi}\int_a^b \left[\frac{1}{2}K(\vec{\nabla}\psi(\rho,\theta))^2 + \frac{1}{2\rho^2}\varepsilon_a\widetilde{\mathcal{C}}^2\psi^2(\rho,\theta)\right]\rho\, d\rho d\theta \\ &+ \int_0^{2\pi}\left\{\frac{W_a}{2}[\psi(a,\theta)-\Phi_a(\theta)]^2 + \frac{W_b}{2}[\psi(b,\theta)-\Phi_b(\theta)]^2\right\}d\theta \\ &+ \int_0^{2\pi}\int_a^b \left[\frac{K}{\rho^2}\left(2\frac{\partial}{\partial\theta}\psi(\rho,\theta)+1\right)\right]\rho\, d\rho\, d\theta, \end{aligned} \tag{3}$$

where W_a and W_b in the second integral refer to anchoring energy in the cylinders of radius a and b, respectively, and $\Phi_{a|b}$ are the angles defining the easy axes in each cylindrical surface. Before to proceed, it is interesting to note that the last term of (3) does not contribute for the Euler-Lagrange equation. By minimizing the above equation, we find that the tilt angle profile of this sample is governed by the following equation

$$\nabla^2\psi(r,\theta) - \frac{\gamma^2}{r^2}\psi(r,\theta) = 0, \tag{4}$$

subjected to the boundary condition

$$+L_b\frac{\partial\psi(r,\theta)}{\partial r} + \psi(r,\theta)|_{r=\beta} = \Phi_b(\theta) \quad \text{and} \quad -L_a\frac{\partial\psi(r,\theta)}{\partial r} + \psi(r,\theta)|_{r=\alpha} = \Phi_a(\theta), \tag{5}$$

where $L_{a,b} = K/(W_{a,b}(b-a))$ are the extrapolation lengths. The Eq. (4) is a simplified form of the equation obtained from Eq. (3) by performing the change of variables $r = \rho/(b-a)$, $\alpha = a/(b-a)$ and $\beta = b/(b-a)$. In addition, $\gamma^2 = \pi^2(E_0/E_c)^2$, where $E_0 = \widetilde{\mathcal{C}}/(b-a)$ and $E_c^2 = \pi^2 K/\varepsilon_a(b-a)^2$ corresponds to the threshold field for the Fréedericksz transition in a sample of slab shape whose thickness is $(b-a)$, in the strong anchoring situation at the surfaces [8]. In order to solve Eq. (4), subjected to the conditions indicated above, we may use the procedure based on separation of variables to reduce the problem of solving a partial differential equation to the one of solving ordinary differential equations. In this direction, we note that the solution may be expanded in terms of the eigenfunctions of the spatial operator of Eq. (4), i.e., $\partial_\theta^2 \Theta_n = -k_n^2 \Theta_n$, after applying the procedure of separation of variables. For this case, the solution can be written as

$$\psi(r,\theta) = \sum_{n=0}^{\infty} \left(\widetilde{\mathcal{A}}_n(r)\Theta_n^+(\theta) + \widetilde{\mathcal{B}}_n(r)\Theta_n^-(\theta) \right) \tag{6}$$

with $\Theta_n^+(\theta) = \cos(m\theta)$ and $\Theta_n^-(\theta) = \sin(m\theta)$. The functions $\widetilde{\mathcal{A}}_n(r)$ and $\widetilde{\mathcal{B}}_n(r)$ are determined by substituting the above solution in Eq. (4) and by taking the orthogonality property of the eigenfunctions and the boundary conditions into account. This manner, the solution for Eq. (4), subjected the boundary conditions given by Eq. (5), is given by

$$\begin{aligned}\psi(r,\theta) = {} & \frac{\Delta_0 r^\gamma - \delta_0 r^{-\gamma}}{2\pi(\Delta_0\sigma_0 - \eta_0\ \delta_0)} \int_0^{2\pi} d\overline{\theta}\Phi_b(\overline{\theta}) + \frac{\sigma_0 r^{-\gamma} - \eta_0 r^\gamma}{2\pi(\Delta_0\sigma_0 - \eta_0\delta_0)} \int_0^{2\pi} d\overline{\theta}\Phi_a(\overline{\theta}) \\ & + \sum_{m=1}^{\infty} \frac{\cos(m\theta)}{\pi(\Delta_m\sigma_m - \eta_m\delta_m)} \int_0^{2\pi} d\overline{\theta}\cos(m\overline{\theta}) f_{ab}(\overline{\theta}) \\ & + \sum_{m=1}^{\infty} \frac{\sin(m\theta)}{\pi(\Delta_m\sigma_m - \eta_m\delta_m)} \int_0^{2\pi} d\overline{\theta}\sin(m\overline{\theta}) f_{ab}(\overline{\theta}),\end{aligned} \tag{7}$$

where

$$f_{ab}(\overline{\theta}) = \Phi_b(\overline{\theta})\left(\Delta_m r^{\xi_m} - \frac{\delta_m}{r^{\xi_m}} \right) + \Phi_a(\overline{\theta})\left(\frac{\sigma_m}{r^{\xi_m}} - \eta_m r^{\xi_m} \right), \tag{8}$$

and

$$\begin{aligned} \delta_0 &= \left(\alpha^\gamma - \gamma L_a \alpha^{\gamma-1}\right), \quad \Delta_0 = \left(\alpha^{-\gamma} + \gamma L_a \alpha^{-(\gamma+1)}\right) \\ \sigma_0 &= \left(\beta^\gamma + \gamma L_b \beta^{\gamma-1}\right), \quad \eta_0 = \left(\beta^{-\gamma} - \gamma L_b \beta^{-(\gamma+1)}\right) \\ \delta_m &= \left(\alpha^{\xi_m} - \xi_m L_a \alpha^{\xi_m-1}\right), \quad \Delta_m = \left(\alpha^{-\xi_m} + \xi_m L_a \alpha^{-(\xi_m+1)}\right) \\ \sigma_m &= \left(\beta^{\xi_m} + \xi_m L_b \beta^{\xi_m-1}\right), \quad \eta_m = \left(\beta^{-\xi_m} - \xi_m L_b \beta^{-(\xi_m+1)}\right), \end{aligned} \tag{9}$$

with $\xi_m = \sqrt{\gamma^2 + m^2}$. In particular, for $L_a = 0$ and $L_b = 0$, Eq. (7) recovers the stationary solution obtained from the time dependent solution found in Ref. [7] for the strong anchoring case. In Figure 2, we present the solution given by Eq. (7)

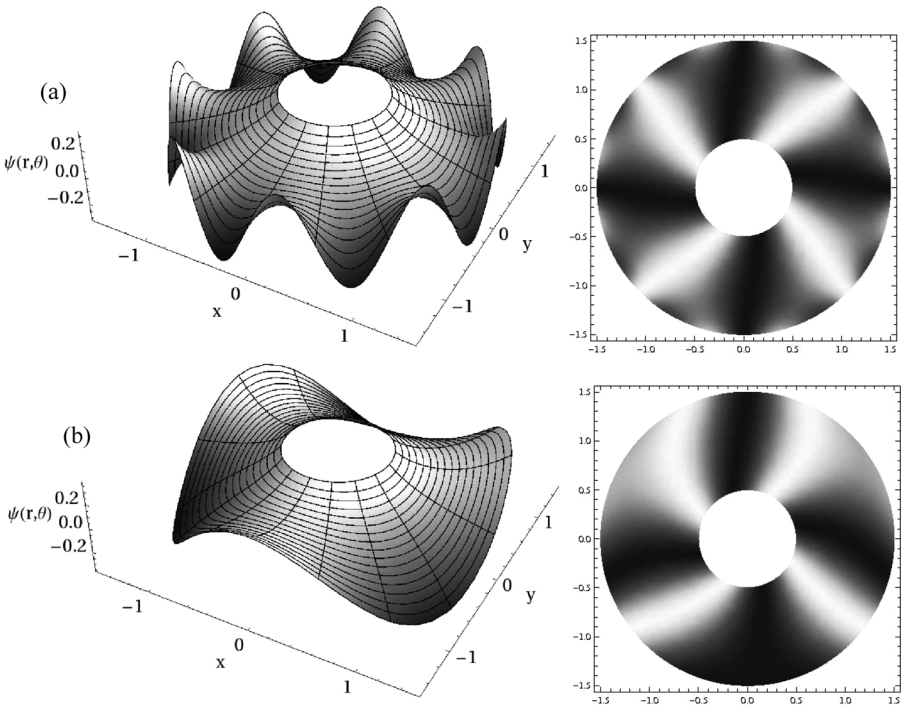

Figure 2. The left figures show the behavior of $\psi(r, \theta)$ (Eq. (7)) whereas the right figures show the simulation of the optical patterns for a sample between crossed polarizer. The Cartesian coordinates used are $x = r\cos(\theta)$, $y = r\sin(\theta)$, $r = \sqrt{x^2 + y^2}$, and $\theta = \arctan(y/x)$, with $\psi(r, \theta) = 0$ for $r \leq \alpha$ or $r \geq \beta$. In (a) (top), we consider $L_a = 0.03\alpha$, $L_b = 0.02\beta$, $\phi_1 = \pi/10$, $\phi_0 = \pi/8$, $\alpha = 0.5$, $\beta = 1.5$ (which implies $b/a = 3$), and $\lambda = \pi/4$. Figure (b) (bottom) was depicted for $\lambda = 3\pi/2$. The other parameters have the same values as in (a). The simulations have been performed for $\gamma = 1$, giving $E_0 = E_c/\pi$.

by considering the surface, located at $r = \alpha$, as having a constant easy axis, i.e., $\Phi_a(\theta) = \phi_0$, and the other one, located at $r = \beta$, with a periodic distribution of the easy axes, i.e., $\Phi_b(\theta) = \phi_1 \sin(q\theta)$, with $q = 2\pi/\lambda$ an integer, and λ being the periodicity of the distribution. In these figures are shown the solutions for two values of λ, in two different views, the 3D and the density plot. The density plot simulates the light intensity that goes through the sample placed between crossed polarizer; these plots have been built using the tool DensityPlot in Mathematica® of the function $\sin^2 2[\Theta(r, \theta)]$ [13], with $\Theta = (\psi(r, \theta) + \theta)$ being the angle between the nematic director and the x-axis. These plots indicate that differently from what happens in a sample of slab shape, even a very small deformation imposed by the surface can produce a noticeable effect on the orientation in a sample in the geometry we are considering. In fact, it is easy to observe that the regular alternating optical pattern corresponding to a uniform orientation is here affected by the very small deformation imposed by the surfaces (as can be shown by the clear deviations from the regular pattern exhibited on the right side of Fig. 2). The 3D plot directly shows the ψ behavior. It is possible to observe that for small values of λ (Fig. 2a), a short range periodic distortion is imposed by the outer surface; on the other hand, when the periodicity increases

(Fig. 2b), we have a long range periodic distortion covering all the sample. If we look at the system with more details, we firstly observe that at those points for which the outer surface imposes to the director a minimum value e.g., $\theta = 3\pi/(2q)$, the tilt angle $\psi(r,\ \theta = 3\pi/(2q))$ presents a zero for some value of r. This point indicates, in some way, how far the distortion imposed by the limiting surface penetrates into the sample. After that, the zeros of the tilt angle have to be searched. If ζ is the zero of the tilt angle for a particular value of λ, it can be interpreted as the length over which the outer surface distortions extends inside the sample, measured from the outer surface, as shown in the inset of Figure 3. One can see that, when λ increases (q vanishes), the distortions extend over a large length. For $q = 0$, there are no zeros because there is no distortion imposed by the surface.

In Figure 4, the relevant case in which one of the surfaces is in the situation of strong anchoring and the other one is in weak anchoring, for typical values of the electric field, is shown. Note that even a small electric field applied to the sample can produce a significant distortion in the sample orientation.

To analyze the problem in the absence of external field, we have to consider Eq. (4) for $\gamma = 0$ and solve the resulting Laplace equation, using again the boundary conditions (5). By following the previous procedure, we have

$$\begin{aligned}\psi(r,\theta) = {} & \frac{\alpha\beta(\ln(\alpha/r) - L_a/\alpha)}{\alpha\beta\ln(\alpha/\beta) - (\beta L_a + \alpha L_b)} \int_0^{2\pi} d\bar{\theta}\Phi_b(\bar{\theta}) \\ & - \frac{\alpha\beta(L_b/\beta + \ln(\beta))}{\alpha\beta\ln(\alpha/\beta) - (\beta L_a + \alpha L_b)} \int_0^{2\pi} d\bar{\theta}\Phi_a(\bar{\theta}) \\ & + \sum_{m=1}^{\infty} \frac{\cos(m\theta)}{\pi(\varsigma\mu - \omega\nu)} \int_0^{2\pi} d\bar{\theta}\cos(m\bar{\theta}) g_{ab}(\bar{\theta}) \\ & + \sum_{m=1}^{\infty} \frac{\sin(m\theta)}{\pi(\varsigma\mu - \omega\nu)} \int_0^{2\pi} d\bar{\theta}\sin(m\bar{\theta}) g_{ab}(\bar{\theta}), \end{aligned} \tag{10}$$

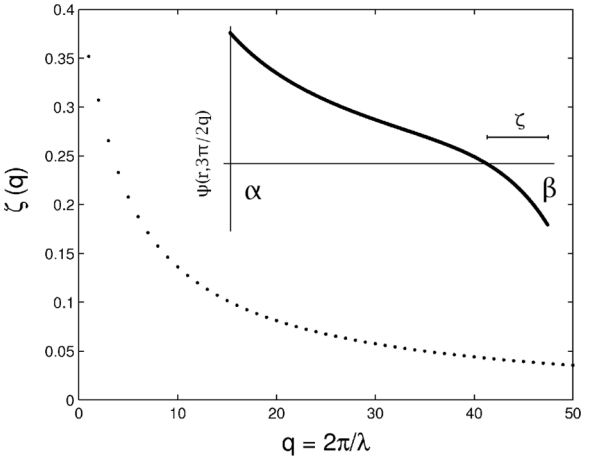

Figure 3. Set of zeros of the tilt angle, ζ, as a function of λ. The inset shows $\psi(r,\ \theta = 3\pi/2q)$, indicating also how ζ is measured. The parameters are the same used in Figure 2.

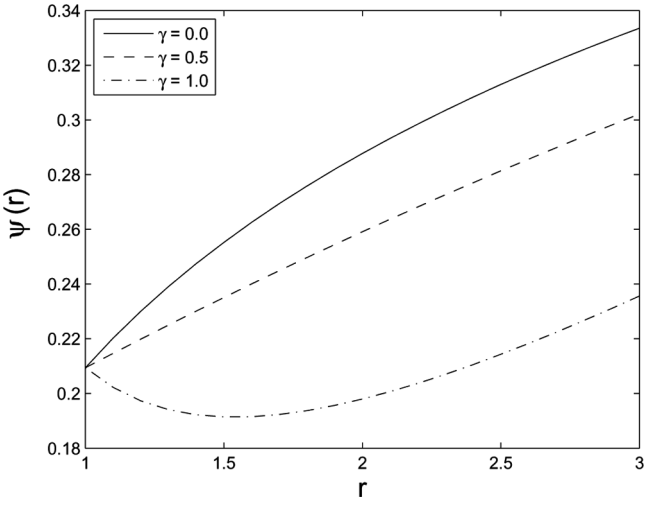

Figure 4. This figure illustrates the behavior of Eq. (7) where for simplicity, we consider $L_a = 0$, $L_b = 12$, $\Phi_a = \pi/15$, $\Phi_b = \pi/4$, $\alpha = 1$, and $\beta = 3$.

where

$$g_{ab}(\overline{\theta}) = \left[\Phi_b(\overline{\theta})\left(\varsigma r^m - \frac{\nu}{r^m}\right) + \Phi_a(\overline{\theta})\left(\frac{\mu}{r^m} - \omega r^m\right)\right], \tag{11}$$

and

$$\begin{aligned} \nu &= \alpha^m - L_a m\alpha^{m-1} \quad \mu = \beta^m + L_b m\beta^{m-1} \\ \varsigma &= \alpha^{-m} + L_a m\alpha^{-(m+1)} \quad \omega = \beta^{-m} - L_b m\beta^{-(m+1)}. \end{aligned} \tag{12}$$

In Figure 5, we show the behavior of $\psi(r, \theta)$ given by solution (10), for representative values of L_b, by considering the inner surface in the situation of strong anchoring in the presence of a homogeneous easy axes distribution.

For the strong anchoring case, i.e., $L_a = 0$ and $L_b = 0$, Eq. (10) yields

$$\begin{aligned} \psi(r,\theta) = &\frac{1}{2\pi\ln(\alpha/\beta)}\left\{\int_0^{2\pi} d\overline{\theta}[\Phi_b(\overline{\theta})\ln(\alpha) - \Phi_a(\overline{\theta})\ln(\beta)] + \ln(r)\int_0^{2\pi} d\overline{\theta}[\Phi_a(\overline{\theta}) - \Phi_b(\overline{\theta})]\right\} \\ &+ \sum_{m=1}^{\infty} \frac{\cos(m\theta)}{\pi[(\beta/\alpha)^m - (\alpha/\beta)^m]} \int_0^{2\pi} d\overline{\theta}\cos(m\overline{\theta})h_{ab}(\overline{\theta}) \\ &+ \sum_{m=1}^{\infty} \frac{\sin(m\theta)}{\pi[(\beta/\alpha)^m - (\alpha/\beta)^m} \int_0^{2\pi} d\overline{\theta}\sin(m\overline{\theta})h_{ab}(\overline{\theta}). \end{aligned} \tag{13}$$

where

$$h_{ab}(\overline{\theta}) = \left[\Phi_b(\overline{\theta})\left(\frac{r^m}{\alpha^m} - \frac{\alpha^m}{r^m}\right) + \Phi_a(\overline{\theta})\left(\frac{\beta^m}{r^m} - \frac{r^m}{\beta^m}\right)\right]. \tag{14}$$

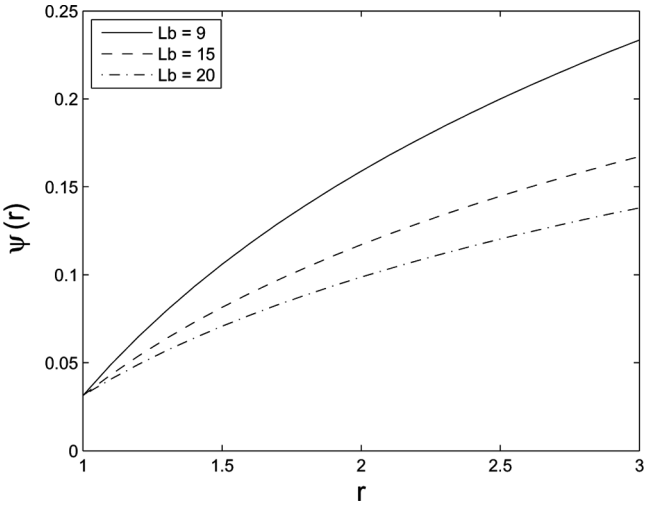

Figure 5. This figure shows the behavior of $\psi(r)$, given by Eq. (10). For simplicity, we consider $L_a = 0$, $\Phi_a = \pi/100$, $\Phi_b = \pi/4$, $\alpha = 1$, and $\beta = 3$.

These profiles are shown in Figure 6. If one considers $\Phi_a = 0$ and $\Phi_b = \text{constant}$, one recovers the same simple results reported in Refs. [4,5].

The previous results are useful, in general, to investigate the splay-bend distortion in liquid crystal when these distortions are small. For this reason, the electrical field must be of the order of the Fréedericksz threshold field to assure that these approximations work well. In addition, they may also be used to obtain the qualitative behaviour of the director when these approximations are relaxed.

In order to complete the analysis, we have performed numerical calculations to solve the complete equation and boundary conditions, for checking the accuracy of the analytical results. The non-linear equation to be solved is

$$\nabla^2\psi(r,\theta) - \frac{\gamma^2}{2r^2}\sin(2\psi(r,\theta)) = 0, \tag{15}$$

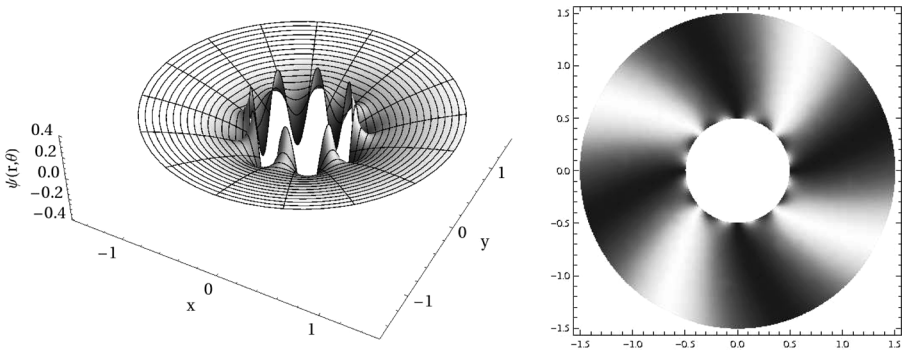

Figure 6. On the left is shown the behavior of $\psi(r, \theta)$, given by Eq. (13), and on the right is shown the simulation of the optical pattern for the sample located between crossed polarizer. We consider $\Phi_b = \pi/8$, $\Phi_a = \pi/10\sin(q\theta)$, $\alpha = 0.5$, $\beta = 1.5$, and $\lambda = \pi/4$.

subjected to the boundary conditions

$$+L_b\frac{\partial\psi(r,\theta)}{\partial r}+\sin(\psi(r,\theta))|_{r=\beta}=\Phi_b(\theta)\quad\text{and}\quad-L_a\frac{\partial\psi(r,\theta)}{\partial r}+\sin(\psi(r,\theta))|_{r=\alpha}=\Phi_a(\theta). \tag{16}$$

In this framework, solutions for Eq. (15) have been searched by means of a standard numerical procedure, essentially based on the Runge-Kutta method [14]. Figures 7a and 7b show the behavior of the tilt angle obtained by using the analytical and numerical calculations for comparative purposes. Note that, depending on the choice of the parameters, we have a good agreement between the analytical and the numerical results. One observes that the agreement is better for large values of the

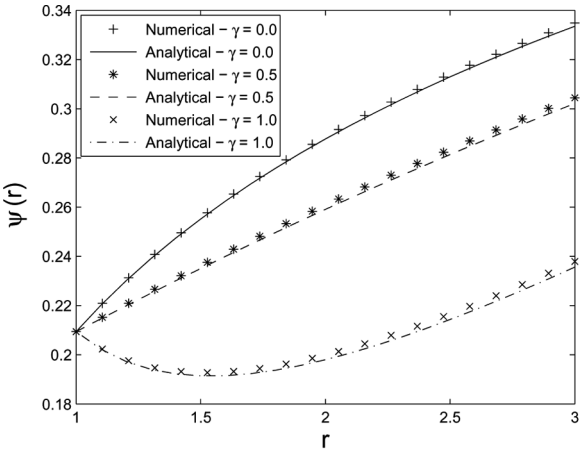

(a)

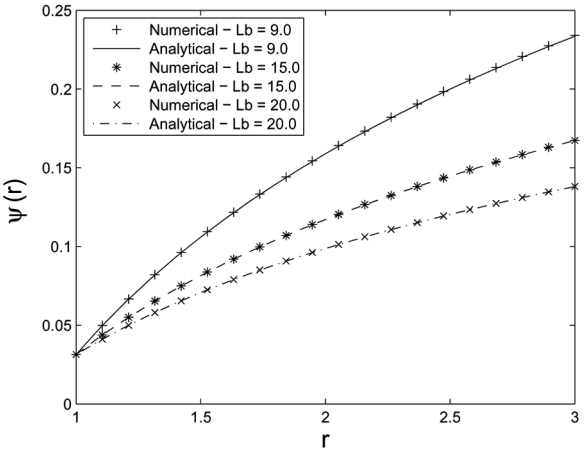

(b)

Figure 7. The analytical and numerical results obtained for the tilt angle are shown in Figures (6a) and (6b). The analytical results are the ones illustrated in Figures (4) and (5). The numerical results are obtained by solving numerically Eq. (15) with Eq. (16).

extrapolation length. This result reinforces the usefulness of the approximations we employ to obtain analytical results for the molecular orientation of nematic samples in different geometries.

III. Conclusions

We have investigated the boundary value problem stated to determine the director profile in a liquid-crystalline sample confined between concentric cylindrical surfaces. We formulate the problem in general terms by considering the presence of an external electric field and easy directions that are θ -dependent. In principle, this situation could be physically relevant for liquid-crystalline systems confined between surfaces that have inhomogeneities in the distribution of easy directions. It was possible to verify that the analytical results are in good agreement with the numerical ones, when the extrapolation length has non vanishing values. The agreement is improved as the extrapolation length increases. On the other hand, although the qualitative behaviour of the director angle in the analytical case seems to be the same as the one numerically obtained, some small discrepancies arise for small values of the extrapolation length because, in this case, the situation approaches the strong anchoring case. The numerical analysis was developed for validating our analytical approach, indicating that even in this approximate case, the tilt angle profile can be determined in a very satisfactory way for a sample in weak anchoring and in the presence of external field.

Acknowledgments

We are grateful to the Brazilian Council of Research (CNPq) for funding R. Teixeira de Souza, E. K. Lenzi, and L. R. Evangelista, and to Coordenadoria de Aperfeiçoamento de Pessoal de Nvel Superior (CAPES) for funding C. A. R. Yednak and G. G. Lenzi.

References

[1] Kotov, I. V., Khazimullin, M. V., & Krekhova, A. P. (2001). *Molecular Crystals and Liquid Crystals*, *366*, 2737–2744.
[2] Tsuru, H. (1990). *Journal of the Physical Society of Japan*, *59*, 1600–1616.
[3] Williams, D. R. M., & Halperin, A. (1993). *Phys. Rev. E*, *48*, R2366.
[4] de Gennes, P. G., & Prost, J. (1993). *The Physics of Liquid Crystals*, 2nd Ed., Clarendon Press: Oxford, 158.
[5] Williams, D. R. M. (1994). *Phys. Rev. E*, *50*, 1686.
[6] Teixeira de Souza, R., Dias, J. C., Mendes, R. S., & Evangelista, L. R. (2009). *Physica A*, *389*, 945–950.
[7] Yednak, C. A. R., Lenzi, E. K., & Evangelista, L. R. (2009). *Braz. J. Phys.*, *39*(2), 312–317.
[8] Barbero, G., & Evangelista, L. R. (2001). *An Elementary Course on the Continuum Theory for Nematic Liquid Crystals*, World Scientific: Singapore.
[9] Stewart, I. W. (2004). *The Static and Dynamical Continuum Theory of Liquid Crystals*, Taylor and Francis: London.
[10] Yednak, C. A. R., Igarashi, R. N., Lenzi, E. K., & Evangelista, L. R. (2006). *Phys. Lett. A*, *358*, 31.

[11] Rapini, A., & Papoular, M. J. (1969). *J. Physique Coll. 30*, *C4*, 54.
[12] Stewart, I. W. (2004). *The Static and Dynamic Continuum Theory of Liquid Crystals*, Taylor & Francis: London.
[13] Loh, K. K., Krauss, I., & Meyer, R. (2000). *Phys. Rev. E*, *62*, 5115.
[14] Shampine, L. F. (1994). *Numerical Solution of Ordinary Differential Equations*, Chapman & Hall/CRC: New York.